Agricultural and Forest Meteorology 213 (2015) 226–239

Contents lists available at ScienceDirect

Agricultural and Forest Meteorology

journal homepage: www.elsevier.com/locate/agrformet

A comparison of optical and microwave scintillometers with eddy covariance derived surface heat fluxes

Mei Sun Yee[a,*], Valentijn R.N. Pauwels[a], Edoardo Daly[a], Jason Beringer[b,c], Christoph Rüdiger[a], Matthew F. McCabe[d], Jeffrey P. Walker[a]

[a] Department of Civil Engineering, Monash University, Clayton, Australia
[b] School of Geography and Environmental Science, Monash University, Clayton, Australia
[c] School of Earth and Environment, University of Western Australia, Crawley 6009, WA, Australia
[d] Division of Biological and Environmental Sciences and Engineering King Abdullah, University of Science and Technology, Thuwal, Saudi Arabia

ARTICLE INFO

Article history:
Received 4 April 2015
Received in revised form 12 June 2015
Accepted 15 July 2015

Keywords:
Evapotranspiration
Eddy-covariance
Scintillometer
Sensible heat
Latent heat

ABSTRACT

Accurate measurements of energy fluxes between land and atmosphere are important for understanding and modeling climatic patterns. Several methods are available to measure heat fluxes, and scintillometers are becoming increasingly popular because of their ability to measure sensible (H) and latent (L_vE) heat fluxes over large spatial scales. The main motivation of this study was to test the use of different methods and technologies to derive surface heat fluxes.

Measurements of H and L_vE were carried out with an eddy covariance (EC) system, two different makes of optical large aperture scintillometers (LAS) and two microwave scintillometers (MWS) with different frequencies at a pasture site in a semi-arid environment of New South Wales, Australia. We used the EC measurements as a benchmark. Fluxes derived from the EC system and LAS systems agreed ($R^2 > 0.94$), whereas the MWS systems measured lower H (bias ~60 W m^{-2}) and larger L_vE (bias ~65 W m^{-2}) than EC. When the scintillometers were compared against each other, the two LASs showed good agreement of H ($R^2 = 0.98$), while MWS with different frequencies and polarizations led to different results. Combination of LAS and MWS measurements (i.e., two wavelength method) resulted in performance that fell in between those estimated using either LAS or MWS alone when compared with the EC system. The cause for discrepancies between surface heat fluxes derived from the EC system and those from the MWS systems and the two-wavelength method are possibly related to inaccurate assignment of the structure parameter of temperature and humidity. Additionally, measurements from MWSs can be associated with two values of the Bowen ratio, thereby leading to uncertainties in the estimation of the fluxes. While only one solution has been considered in this study, when L_vE was approximately less than 200 W m^{-2}, the alternate solution may be more accurate. Therefore, for measurements of surface heat fluxes in a semi-arid or dry environment, the optical scintillometer is recommended, whereas further work will be required to improve the estimation of surface heat fluxes from microwave systems.

1. Introduction

The ability to quantify the energy and mass exchange between the land surface and the atmosphere is important for improving models used in water resource management. Field measurements of sensible heat (H) and latent heat (L_vE) are also crucial for the validation of remote sensing surface heat flux products (Brunsell et al., 2011; Fritschen et al., 1992; Jung et al., 2009; Kite and Droogers, 2000).

The most popular approach adopted to measure surface heat fluxes is based on the eddy-covariance (EC) method (Kaimal and Finnigan, 1994), with EC systems deployed globally through the FLUXNET network (Baldocchi et al., 2001; Maayar et al., 2008). However, as the footprint of EC systems changes with meteorological conditions, its representativeness of model grids and satellite pixels, particularly in a heterogeneous landscape, is debatable (Ward et al., 2014). Scintillometry presents an alternative method, as meteorological changes have little impact on its footprint and it is able to measure path integrated fluxes ranging from a few hundred meters to 10 km (Baghdadi et al., 2007; Beyrich et al., 2002; Meijninger and De Bruin, 2000; Samain et al., 2011), thereby making it more suitable for long-term validation of model simulations

* Corresponding author.
E-mail address: mei.yee@monash.edu (M.S. Yee).

http://dx.doi.org/10.1016/j.agrformet.2015.07.004

and remotely sensed surface heat flux products (Hemakumara et al., 2003; Hendrickx et al., 2007).

A scintillometer consists of a transmitter that emits electromagnetic wave signals to a receiver, which records the intensity of this signal from a distance. As the signal propagates through the atmosphere toward the receiver, it is scattered by turbulent eddies in the atmosphere. This scattering is detected as fluctuations in the intensities of the signal recorded by the scintillometer's receiver (i.e., scintillations). These eddies are driven by surface forcing, such as wind shear from frictional drag of winds flowing over the ground, heat fluxes from the ground caused by solar incident radiation, and turbulent wakes from obstacles like trees (Stull, 1988). Consequently, by combining theoretical principles of atmospheric turbulence with the physics of electromagnetic wave propagation, surface heat fluxes can be derived (e.g., Van Kesteren, 2012).

The turbulence causing scintillations in the atmosphere can be quantified by the structural parameter of the refractive index, C_n^2, and are mainly affected by the structural parameters of temperature, C_T^2, humidity, C_Q^2, and the cross structural parameter of temperature and humidity, C_{TQ} (Kohsiek, 1982). C_T^2 is directly related to H whereas C_Q^2 is directly related to L_vE. Temperature fluctuations given by C_T^2 are the dominant cause of scintillation in the optical wavelengths, and therefore optical scintillometers can be applied to measure H without making measurements of, or assumptions on, humidity fluctuations. Commercially available optical scintillometers have been widely used and have shown to perform similarly to Bowen ratio energy balance (BREB) techniques, hydrological models, and satellite and EC measurements over different types of landscapes (e.g., Brunsell et al., 2011; Chehbouni et al., 2000; Ezzahar et al., 2009; Lagouarde et al., 2002; Liu et al., 2013; McJannet et al., 2011; Meijninger et al., 2002, 2002; Pauwels et al., 2008; Savage, 2009; Samain et al., 2011, 2011, 2012; Zeweldi et al., 2010), including open water and urban areas (Samain et al., 2011; McJannet et al., 2013; Lagouarde et al., 2006; Ward et al., 2013).

Conversely, no wavelengths have been identified in which C_Q^2 is most dominant. Therefore, to derive C_Q^2, the microwave (or millimeter wave) scintillometer (MWS), which is sensitive to both humidity and temperature fluctuations, can be used in combination with an LAS by making assumptions on the value of r_{TQ} (e.g., Evans, 2009; Meijninger et al., 2002) or measuring r_{TQ} based on the bichromatic correlation method (Beyrich et al., 2005; Lüdi et al., 2005; Ward et al., 2015, 2015). The combined use of MWS and LAS is commonly referred to as the two-wavelength method. As for MWS systems, they were not used independently until Kohsiek and Herben (1983) derived surface heat fluxes using a standalone MWS (frequency, f = 30 GHz) by making assumptions regarding r_{TQ} and the Bowen ratio (β). Leijnse et al. (2007) showed that by introducing the energy budget constraint to derive the surface heat fluxes, the standalone MWS (f = 27 GHz) can be used to measure H and L_vE in relatively moist environments. Given the success of LAS in measuring area-averaged H, the possibility of using a standalone MWS in the same way to measure area-averaged L_vE is undeniably attractive. However, to this date, no studies using the two-wavelength method or a standalone MWS have been carried out in a semi-arid environment. Due to differences in the frequencies used in different studies, it is also of value to understand the effect this might have on the measurements.

Consequently, the aim of this study is to test the application of scintillometers to measure H and L_vE in a semi-arid environment. Here, the results from comparing an EC system with two different LAS manufacturers, Kipp and Zonen (LAS) and Scintec (BLS 900) (herein referred to as Kipp and Scintec, respectively), two MWSs with f of 26 GHz and 38 GHz (herein referred to as MW26 and MW38, respectively) and two polarizations (horizontal, h and vertical, v), and different combinations of LAS and MWS in the two-wavelength method, are presented.

2. Methods

2.1. Site description

The site of this intercomparison is located in the Yanco Study Area (contained between 34.56° S and 35.17° S, and 145.83° E and 146.4° E) (Fig. 1), which is situated within the western plains of the Murrumbidgee River catchment, in New South Wales, Australia (Smith et al., 2012). According to data from 1981 to 2010 (Bureau of Meteorology station ID. 074037), the daily mean temperatures vary significantly from 34.0 °C in January to 14.2 °C in July. Mean annual rainfall is 418.5 mm and is distributed relatively evenly across all months. The dominant wind directions are from the south-west and north-east. The site consists of a homogeneous flat grassland that is used for the grazing of cattle; the grassland is dominated by perennial tussock grasses, such as kangaroo and wallaby grasses (Natural Resources Advisory Council, 2010). The soil type is sand over clay (loamy sand) and typical porosity of this soil type is about 0.30 m^3 m^{-3} (Hornbuckle and Christen, 1999; Smith et al., 2012).

2.2. Measurement description

The EC system was mounted on a 20 m tower (located at 34.99° S and 146.30° E) at 6 m above the ground, and has been in operation since May 2012. The EC system consists of a CSAT3 3-D sonic anemometer (Campbell Scientific, Inc.) and a LI-7500 open path infrared gas analyzer (IRGA) (LI-COR Inc., U.S.) with a sampling frequency of 10 Hz following the general approach of Beringer et al. (2007) and Hutley et al. (2005).

In November 2012, the two LAS systems, Kipp and Scintec, were deployed along a 1 km path (L) (Fig. 1). The receivers were situated about 1 km west of the EC tower and the transmitters were installed approximately 10 m from the foot of the EC tower (Fig. 1). Due to complexity of setting up multiple towers within a flat and remote open area, both LAS systems were set up with an effective beam height, z_s, of 2.50 m. Despite the seemingly low height, due to the success of other studies in using scintillometers below blending height (e.g., Ezzahar et al., 2007; Meijninger et al., 2002), and the homogeneity and low vegetation height (<0.30 m) at the site, this is deemed to be acceptable. To avoid interference, the two LAS transmitters were installed approximately 250 m apart. The 1-min values of C_n^2, computed internally by the LAS systems provided by the manufacturers, were used to derive H and L_vE.

The two MWS systems, MW26 and MW38, were deployed in November 2013 between the two LAS systems. Both MWS systems also have an effective beam height of 2.50 m. The MWS transmitters transmit signals rotated from the horizontal plane by 45° to allow splitting by an ortho-mode transducer on the receiver antenna into identical h and v polarization receiver channels. The raw voltages measured at 10 Hz frequency by the MWS receivers were converted to intensities, I, as provided by the manufacturer of the MWS system. To avoid absorption effects, the lower cut-off frequency for the MWS was 0.03 Hz respectively (Green et al., 2001). Values of C_n^2 every minute were calculated from the intensities as

$$C_n^2 = \frac{2^{14/3}\Gamma(7/3)\cos(\pi/12)}{\pi\sqrt{3\pi}\,\Gamma(8/3)} k^{-7/6} L^{-11/6} \sigma^2_{\ln(I)}, \quad (1)$$

where $\Gamma(\cdot)$ is the gamma function and $k = 2\pi/\lambda$ is the wave number of the electromagnetic wave and its wavelength, λ (Leijnse et al., 2007).

Net radiation (R_n) was derived from incoming and outgoing short- and long-wave radiation measured using two CMP-21

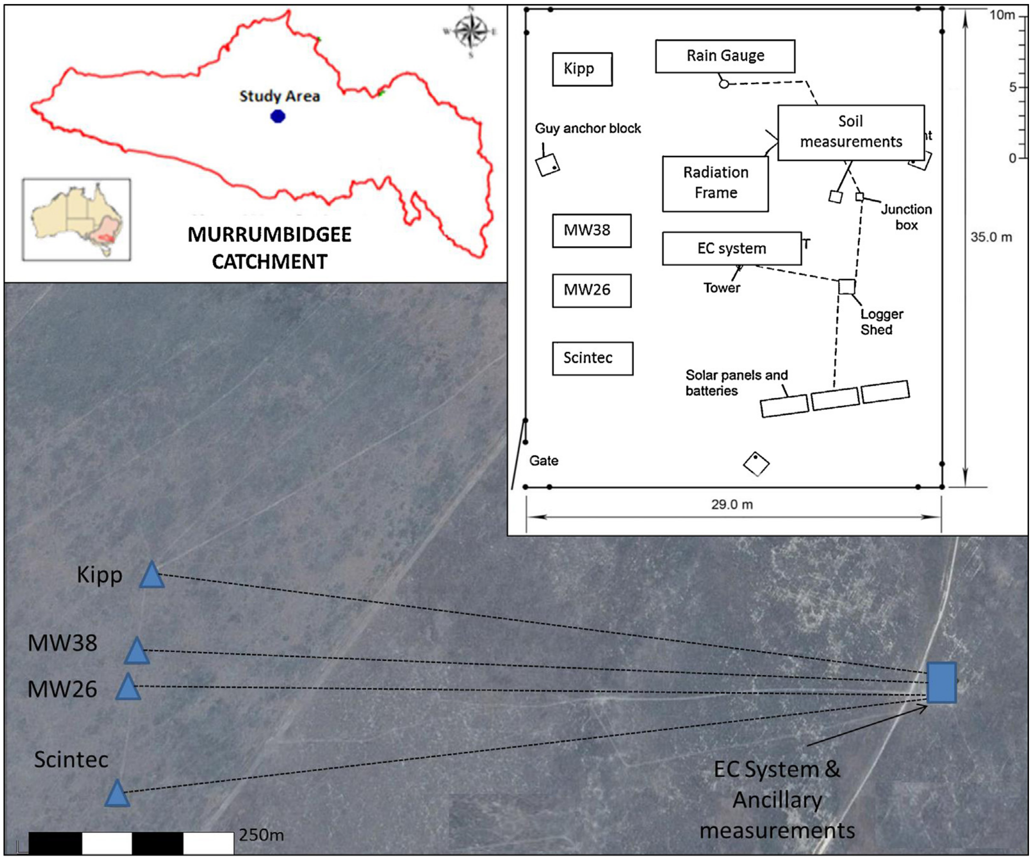

Fig. 1. Layout of the experimental site. Dotted lines indicate the propagation paths of the transmitters' signal to the receivers which are located close to the EC tower. Left inset: Location of the study area within the Murrumbidgee River catchment. Right inset: Plan view of the EC system site with locations of the CSAT and IRGA on the tower, scintillometer receivers, frame mounted radiometers, soil measurement plot, and other ancillary measurements.

Pyranometers and two CRG-4 Pyrgeometers (Kipp and Zonen), which were installed in a standalone configuration approximately 13 m north-east of the EC system and 2 m above the soil surface (Fig. 1). Ground heat flux (G) was determined by combining measurements from soil heat flux plates (Hukseflux HFP01) buried at a depth of 7 cm, and soil temperature (PT-100 Soil Temperature Sensor) and moisture probes (TRIME-PICO 32) at 3 cm and 10 cm depth. Soil volumetric heat capacity, C_s, was calculated using a site specific linear regression (Lukowski, personal communication) derived from in-situ measurements which reads,

$$C_s = 0.06\theta + 1.21, \tag{2}$$

where θ is the soil volumetric content. Eq. (2) was derived using measurements of C_s, soil temperature and soil moisture from 95 samples across the Murrumbidgee catchment. Additionally, a weather station, which measured wind speed (u) and direction (2 m above ground, z_u), air temperature (T), pressure (P), humidity (Q) and precipitation, was installed next to the Scintec. Averages of these measurements were recorded every 10-min as well as the rainfall totals. These data were transformed into 30-min averages and rainfall totals to be combined with data from the scintillometers and calculate H and L_vE. The campaign period for this study was from the 23rd of November 2013 to the 18th of February 2014 (end of spring to summer in the southern hemisphere). The roughness length, z_0, and the displacement height, d_0, were calculated as shown in Eq. (A.9) using a vegetation height value, h_0, of 0.3 m.

2.3. Data analysis

Only daytime data (i.e., unstable conditions) were used in the analysis. Stable and unstable conditions were determined based on Monin–Obukhov length (L_{Ob} [m]) derived from the EC system. During a rainfall event, measurements taken between 30-min before and after the event were not considered. The time-window was selected to account for the distance between the scintillometers and the rain gauge, which can generate lags between times of precipitation at the locations of the rain gauge and scintillometers.

The surface heat fluxes derived from all sensors were averaged to 30-min. To compare H and L_vE derived from different sensors, a orthogonal regression was performed for each pair of sensors to derive the slope and intercept of the line. Additionally, Root Mean Square Difference (RMSD), coefficient of determination (R^2) and bias ($\bar{x} - \bar{y}$) were also computed. The sensor specific processing steps that have been carried out are summarized in the following sections.

2.3.1. Eddy covariance

These data were processed using the software EddyPro (version 5.2.1) to calculate average fluxes at 30-min intervals. The corrections implemented in the analysis included spike detection and removal, lag correction relative to the vertical wind component based on covariance maximization method, linear detrending, sonic virtual temperature correction, coordinate rotation using the double rotation method, spectral corrections for low and high pass filtering effects (Moncrieff et al., 2005) and the Webb–Pearman–Leuning correction (Webb et al., 1980).

2.3.2. Scintillometers

The method used to convert the scintillometer measurements to surface heat fluxes follows that of Leijnse et al. (2007) and is summarized in Appendix A. MWS systems are sensitive to both temperature and humidity fluctuations; the same measurement of C_n^2 can lead to two different values of β, and thus H and L_vE (Leijnse et al., 2007; Ward et al., 2015). For common atmospheric conditions in temperate climates, one solution, β_1, is typically below 2.5 whereas the other, β_2, is larger than 2.5. The smaller β solution will be referred to as β_1, and the larger as β_2. Only the surface heat fluxes derived from β_1 are shown in the results as, for the majority of the time, β_2 was unrealistically large. However, it is important to be aware of the existence of β_2 as this will be referred to in the discussion section.

As Evans (2009) and Ward et al. (2015) observed under and over-closure of energy balance based on measurements from the two-wavelength method, to ensure closure of the energy balance, β derived from the scintillation measurements were used to scale scintillometer derived fluxes proportionally up or down to meet the total available energy, $R_n - G$. Analysis carried out by varying r_{TQ} between 0.8 and 1 showed that the performance of the scintillometers did not change substantially. For this reason, r_{TQ} was assumed to be 1 here. Details of the procedure used to derive H and L_vE from the two-wavelength method can also be found in Appendix A.

In addition to the two LAS and four MWS outputs, in the two-wavelength method, eight possible combinations of LAS and MWS outputs have been used to derive surface heat fluxes, thereby yielding a total of 14 derived H and L_vE estimates from scintillometers at 30-min time-steps. To differentiate the results, subscripts are used to denote the scintillometer used to derive H or L_vE from standalone scintillometers according to ‘K’ (Kipp) or ‘S’ (Scintec) or frequency such as ‘26’ (26 MHz) or ‘38’ (38 MHz) followed by polarization ‘h’ (horizontal) and ‘v’ (vertical) for the MWS. For example, H derived from Kipp is annotated as H_K, and L_vE derived from the h-polarization of MW26 is referred to as L_vE_{26h}. For the two-wavelength method, the optical scintillometer used is denoted as the subscript and the MWS used as the superscript (e.g., $L_vE_K^{38v}$).

3. Results and discussion

In general, H_{EC} was the dominant surface heat flux, whereas L_vE_{EC} remained lower than 200 W m^{-2} for most of the study period. Low soil water availability during the study period was likely the cause of this (<0.10 m^3 m^{-3} for most of the period). Moreover, vegetation at the site was visibly suffering water stress and soils were beginning to crack. Bowen ratio averaged approximately 4 throughout the study period based on measurements from the EC system, 2 based on LAS systems, varying from 0.4 to 1.5 based on β_1 and 5.5 to 20 for β_2 of MWS systems. In semi-arid environments, β is around 4 and can increase to around 15 (Beringer et al., 2007).

3.1. Energy balance closure of EC system

Consistent with the energy balance closure observed in many studies, the orthogonal regression for the energy balance of the EC system, calculated using 30-min averages, was found to have a slope of 0.79 and an intercept of 11.15 W m^{-2}, with an RMSD of 93.60 W m^{-2} (Fig. 2). Possible causes for this may be attributed to errors in measurements of R_n and G, and in turbulent fluxes from the sonic anemometer, energy losses unaccounted for during stable conditions, advection and inadequate accounting of other storage terms (Foken, 2008; Leuning et al., 2012; Wilson et al., 2002). Additionally, as the soil moisture and soil parameters used to derive soil heat storage were from a single point, the estimated soil heat storage may not be representative of the study area. Errors in the

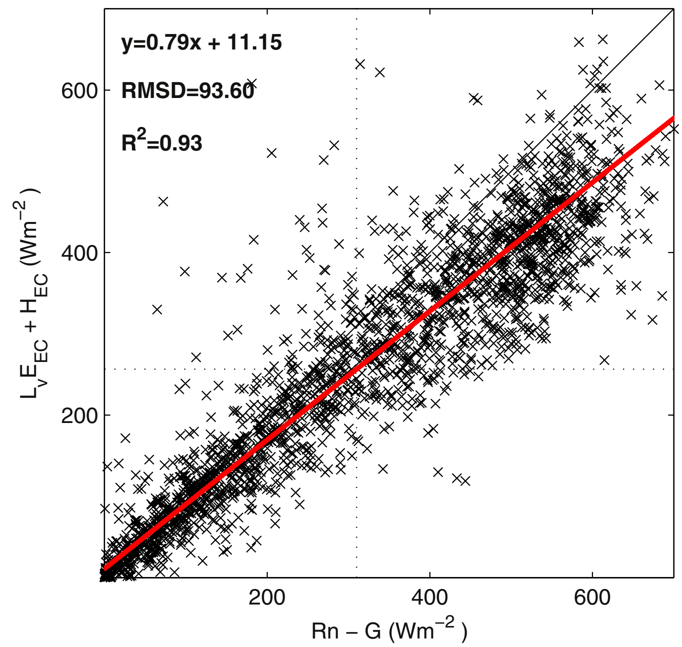

Fig. 2. Energy balance closure of EC station. Solid black line: 1:1 line. Solid red line: fitted line from orthogonal regression. Dotted black lines: mean of $(R_n - G)$ and $(L_vE_{EC} + H_{EC})$. (For interpretation of the references to color in this figure legend, the reader is referred to the web version of this article.)

computation of available energy will also affect the magnitude of surface heat fluxes derived from scintillometry.

3.2. Comparison between EC and scintillometers

3.2.1. Sensible heat

H values derived from the scintillometers were compared to H_{EC}. The results are given in Fig. 3 and Table 1. While H from the LAS systems were very similar to H_{EC}, especially for lower values of H, a wider scatter was observed when H was larger than approximately 350 W m^{-2}. Regarding the MWS systems, this wider scatter as H increases is also apparent. Moreover, results from MW38 were closer to the EC system than MW26. Due to site restrictions, the measurement height of MW26 and MW38 were not much smaller than their Fresnel zones; approximately 2.8 m and 3.4 m respectively. As a result, a portion of turbulent fluctuations may have been missed due to outer scale effects thereby underestimating C_n^2 by up to 5–10%. The performance of MWS improved when using the two-wavelength method.

Similarity theory adopted by scintillometry to enable the derivation of surface heat fluxes assumes that the turbulent transport of heat and water vapour is similar. However, the diffusivity of heat has been shown to be typically higher than water vapour in a semi-arid grassland (Alfieri et al., 2009). Furthermore, it is assumed in this paper that the structure parameter of temperature and humidity are perfectly correlated (r_{TQ} = 1, in Eq. (A.13)), but lower values have been used in some studies (Lüdi et al., 2005). Ward et al. (2015) have also shown that the choice of similarity function can alter daily ET by more than 15–20%, possibly leading to an underestimation of H from the LAS systems compared to that from the EC system. Moreover, studies have shown that uncertainty in h_0 can lead to inaccuracy in the derived fluxes (Evans and De Bruin, 2011; Hartogensis et al., 2003). In this study, h_0 was assumed to be constant. While the study area was flat, an inaccurate assignment of h_0 could impact the estimation of the heat fluxes, since $(z_s - d_0)$ determines the scaling, and therefore the magnitude, of

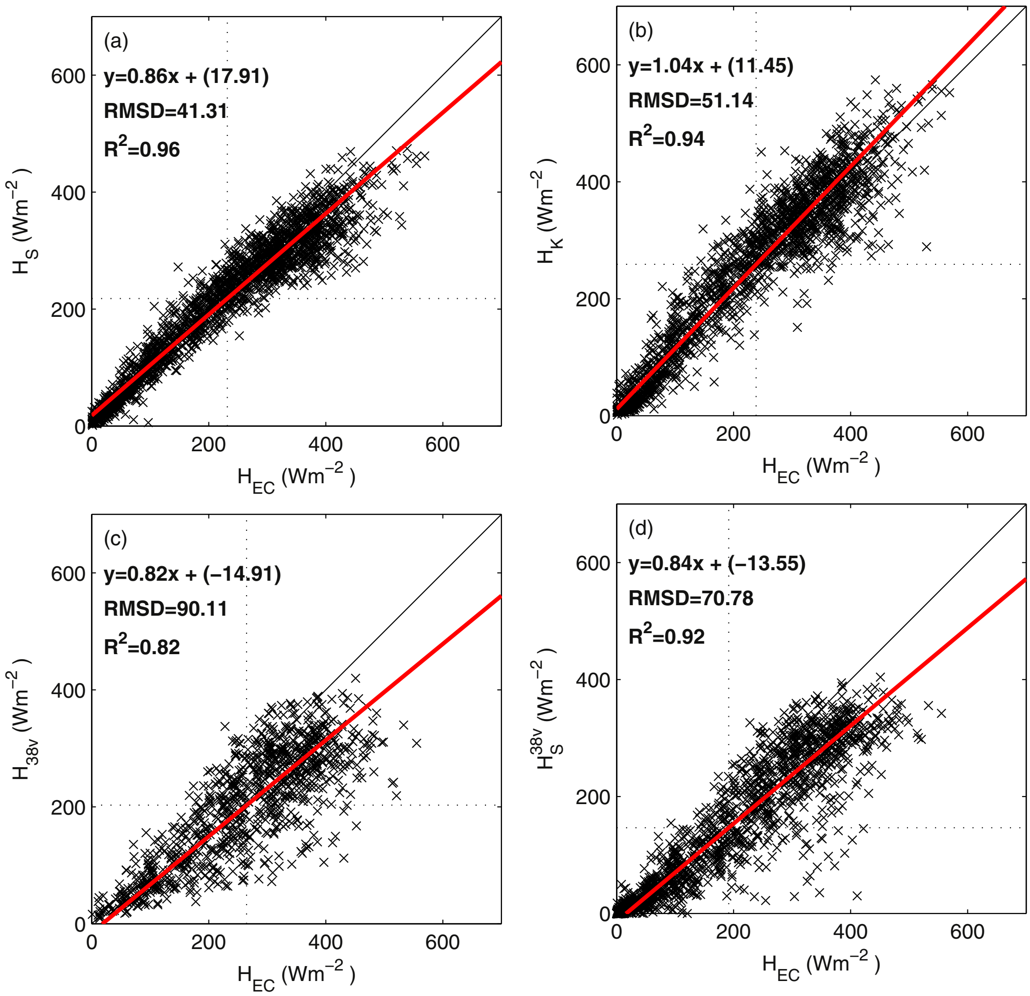

Fig. 3. Comparison of H derived from (a) Scintec, (b) Kipp, (c) MW38v, and (d) MW_S^{38v} with H measured by the EC system. Solid black line: 1:1 line. Solid red line: fitted line from orthogonal regression. Dotted black lines: mean H of each corresponding system. (For interpretation of the references to color in this figure legend, the reader is referred to the web version of this article.)

H and L_vE (Eqs. (A.10) and (A.12)). The above uncertainties likely explain systematic differences in Fig. 3.

3.2.2. Latent heat

Comparison between L_vE_{EC} and L_vE from the scintillometers showed very low correlations (R^2 between 0.37 and 0.53) (Fig. 4, left side). The derived slopes ranged from 3.19 to 4.44, thereby indicating that L_vE from the scintillometers were significantly higher than L_vE_{EC}. Since H between the EC system and scintillometers agreed well, the discrepancy between L_vE_{EC} and L_vE from the scintillometers can be partly attributed to underestimation of L_vE_{EC} as also observed by Ward et al. (2015).

Since the non-turbulent portion of the energy balance can be measured with higher accuracy, the quality of the turbulent fluxes measured by the EC system and scintillometers can be improved if the energy budget is forced to close. This can be done in two ways: the 'residual-LE closure' method or 'β closure' method (Twine et al., 2000).

In the first method, it is assumed that H is accurately measured, and that the non-closure of the energy balance of the EC system comes from an underestimation of L_vE_{EC}. Therefore, the energy budget was forced to close based on the estimate of L_vE_{EC} derived as a residual from the energy balance (i.e., $LE_{EC}^{Res} = R_n - G - H_{EC}$) (Fig. 4). In the second method, assuming that β derived from the EC system is accurately measured, H and L_vE are adjusted to close the energy balance of the EC system using Eqs. (A.1) and (A.2) (herein referred to as $H_{\beta EC}$ and $L_vE_{\beta EC}$) (Fig. 5).

In-comparison to $H_{\beta EC}$ and $L_vE_{\beta EC}$, LE_{EC}^{Res} show better agreement with the scintillometers. Therefore, the non-closure of the energy balance of the EC system is more likely to come from underestimation of L_vE. When $L_vE_{EC}^{Res}$ was compared with the scintillometers, RMSD reduced to a third and R^2 quadrupled in some cases (Fig. 4, right side). However, when L_vE was approximately less than 200 W m^{-2}, the MWS systems resulted in L_vE consistently larger than $L_vE_{EC}^{Res}$. As mentioned earlier, the sensitivity of scintillometers reduce when β is above 2.5. Also, there are two possible solutions for β when solving for the standalone MWS systems. It was assumed in this study that β_1 was the correct solution. However, as β approaches 2.5 it becomes increasingly uncertain as to which β is more reliable. Moreover, the value of the two solutions get closer to each other as β_1 increases, thereby leading to the large scatter observed at low magnitudes of L_vE (higher β). In addition, r_{TQ} determines the relationship between C_n^2 and β (Eq. (A.13)). Therefore, the accuracy of the β solutions also depend on the accuracy of r_{TQ}. An inaccurate assumption of r_{TQ} would further contribute to the mismatch between heat fluxes derived from the EC system and standalone MWS systems. These field observations agree with the deductions made by Leijnse et al. (2007)

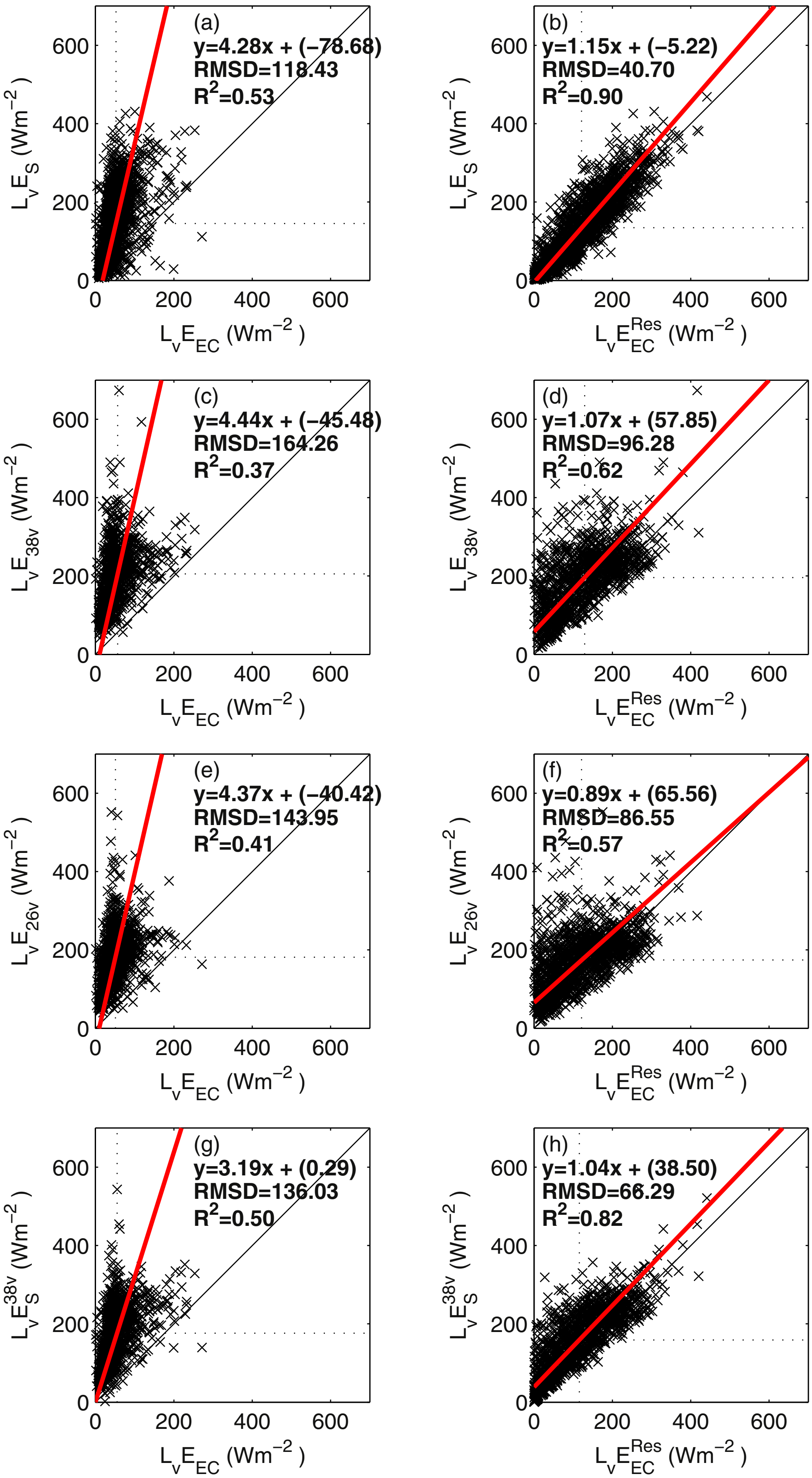

Fig. 4. Comparison of L_vE from (a), (b): Scintec; (c), (d): MW38v; (e), (f) MW26v and (g), (h): MW_S^{38v} with L_vE_{EC} (left column) and $L_vE_{EC}^{Res}$ (right column). Solid black line: 1:1 line. Solid red line: fitted line from orthogonal regression. Dotted black lines: mean L_vE of each corresponding system. (For interpretation of the references to color in this figure legend, the reader is referred to the web version of this article.)

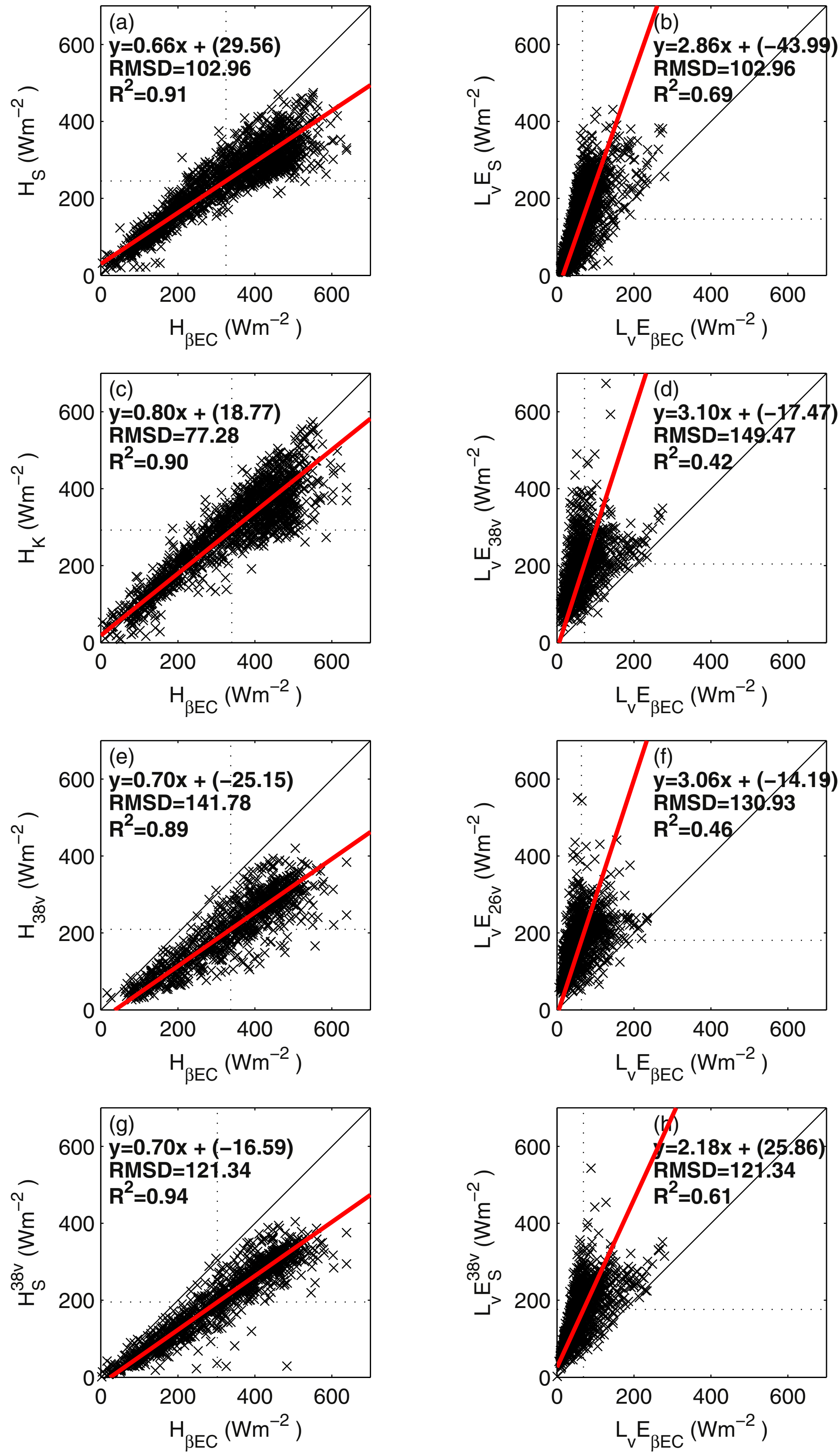

Fig. 5. Comparison of $H_{\beta EC}$ (left column) and $L_vE_{\beta EC}$ (right column) where (a) $H_{\beta EC}$ vs. H_S; (b): $L_vE_{\beta EC}$ vs. L_vE_S; (c) $H_{\beta EC}$ vs. H_K (d): $L_vE_{\beta EC}$ vs. H_{38v}; (e) $H_{\beta EC}$ vs. H_{38v}; (f) $L_vE_{\beta EC}$ vs. L_vE_{26v} (g) $H_{\beta EC}$ vs. H_S^{38v}; and (h): $L_vE_{\beta EC}$ vs. $L_vE_S^{38v}$. Solid black line: 1:1 line. Solid red line: fitted line from orthogonal regression. Dotted black lines: mean L_vE of each corresponding system. (For interpretation of the references to color in this figure legend, the reader is referred to the web version of this article.)

Table 1
Statistics derived from orthogonal regression of H.

Sensor 1 (x)	Sensor 2 (y)	Slope	Intercept	RMSD	R^2	Bias
H_S	H_K	1.20	−6.55	49.06	0.98	−37.80
	H_{38v}	0.99	−43.83	76.76	0.79	45.10
	H_{38h}	0.99	−39.01	73.77	0.81	42.61
	H_{26v}	1.08	−48.70	67.52	0.82	29.42
	H_{26h}	1.03	−68.68	91.03	0.70	61.18
	H_S^{38v}	0.96	−26.09	57.75	0.91	33.87
	H_S^{38h}	0.96	−23.62	55.68	0.92	31.63
	H_S^{26v}	1.02	−28.47	55.06	0.91	23.94
	H_S^{26h}	0.96	−38.16	71.26	0.89	47.95
	H_K^{38v}	0.99	−25.43	54.24	0.92	27.27
	H_K^{38h}	0.99	−22.98	52.36	0.92	25.11
	H_K^{26v}	1.04	−27.41	52.96	0.91	18.42
	H_K^{26h}	0.98	−37.51	66.76	0.90	41.19
H_{38v}	H_{38h}	0.99	5.51	12.11	0.99	−3.43
	H_{26v}	1.08	7.41	36.29	0.96	−23.74
	H_{26h}	1.06	−28.96	38.36	0.91	14.31
	H_K	1.28	22.20	105.36	0.82	−82.56
	H_S^{38v}	0.96	24.01	23.40	0.98	−15.42
	H_S^{38h}	0.96	25.90	26.83	0.98	−17.32
	H_S^{26v}	1.06	19.19	42.26	0.96	−30.53
	H_S^{26h}	1.02	−0.52	31.32	0.95	−3.49
	H_K^{38v}	0.98	26.22	29.69	0.98	−22.87
	H_K^{38h}	0.98	28.04	32.53	0.98	−24.67
	H_K^{26v}	1.08	21.48	47.49	0.96	−36.85
	H_K^{26h}	1.05	2.29	33.39	0.95	−11.42
H_S^{38v}	H_S^{38h}	1.00	1.60	6.88	1.00	−1.97
	H_S^{26v}	1.07	0.28	22.25	0.99	−11.14
	H_S^{26h}	0.99	−8.16	24.29	0.98	9.03
	H_K^{38v}	1.03	1.01	7.72	1.00	−5.38
	H_K^{38h}	1.03	2.58	10.96	1.00	−7.28
	H_K^{26v}	1.10	1.47	25.92	0.99	−15.77
	H_K^{26h}	1.03	−7.05	22.60	0.98	3.40
H_{EC}	H_S	0.86	17.91	41.31	0.96	13.67
	H_K	1.04	11.45	51.14	0.94	−20.38
	H_{38v}	0.82	−14.91	90.11	0.82	61.92
	H_{38h}	0.82	−13.44	86.61	0.84	58.61
	H_{26v}	0.90	−23.64	81.97	0.83	50.02
	H_{26h}	0.79	−23.61	109.84	0.74	83.52
	H_S^{38v}	0.84	−13.55	70.78	0.92	44.84
	H_S^{38h}	0.84	−12.05	69.05	0.93	42.90
	H_S^{26v}	0.88	−14.70	67.21	0.92	38.72
	H_S^{26h}	0.80	−19.91	84.43	0.91	58.70
	H_K^{38v}	0.86	−13.35	67.02	0.92	39.46
	H_K^{38h}	0.87	−11.85	65.39	0.93	37.59
	H_K^{26v}	0.90	−14.22	64.34	0.92	34.19
	H_K^{26h}	0.83	−19.66	79.91	0.91	53.18

regarding the effect that assumptions of r_{TQ} will have towards derived surface heat fluxes. To enable the use of a standalone MWS in semi-arid environments, further studies will need to be carried out.

When additional information is provided to the system of equations, β is no longer a non-unique solution. In this case, scintillometer derived L_vE resulted in more similar to $L_vE_{EC}^{Res}$ with correlations increasing to between 0.77 and 0.82 and slopes of 0.92 to 1.04 (Table 2). A comparison of β derived from the scintillometers and the EC system also showed a diminishing correlation as β approached 2.5 for the MWS systems, whereas correlations with the LAS systems were significantly higher (not shown here). Finally, it cannot be dismissed that the accuracy of the derived surface heat fluxes from the scintillometers are highly dependent on the accuracy of measurements of R_n and G, as the remaining available energy is partitioned into H and L_vE based on β derived from scintillometer measurements.

In this study, while the two-wavelength method performed comparably well, it can be said that the standalone LAS still performs the best when compared with EC for both L_vE and H without the MWS.

3.3. Scintillometer inter-comparison

Here we compare (i) H from standalone LAS from different manufacturers, (ii) L_vE from standalone MWS of the same frequencies but different polarization, (iii) MWS of two different frequencies, and (iv) both H and L_vE from the standalone methods with the two-wavelength method.

It can be seen in Fig. 6 that the correlation between H derived from the two LAS systems was high, 0.98, with an RMSD of 49.06 W m^{-2}. However, H_S was approximately 20% lower than H_K (bias of −37.80 W m^{-2}), which is consistent with results from previous studies (e.g., Kleissl et al., 2009; Solignac et al., 2012; Van Kesteren et al., 2015). They attributed these differences to absorption, and electronic and optical problems of the scintillometers. To reduce the effect of absorption, as in Solignac et al. (2012), the BLS900 from Scintec is recommended due to its ability to correct for absorption based on its dual beam configuration (two different pulse coding frequencies are used). On the other hand, Van Kesteren et al. (2015) found that the equations applied by Scintec to determine (1) the variance of the logarithmically transformed I, $\sigma^2_{\ln(I)}$, and (2) covariance of I from a time series, resulted in an

Table 2
Statistics derived from orthogonal regression of L_vE.

Sensor 1 (x)	Sensor 2 (y)	Slope	Intercept	RMSD	R^2	Bias
L_vE_S	L_vE_K	0.88	−20.60	49.06	0.93	37.80
	L_vE_{38v}	0.89	69.83	88.83	0.65	−53.77
	L_vE_{38h}	0.90	65.61	85.46	0.67	−50.86
	L_vE_{26v}	0.75	69.97	76.60	0.64	−35.78
	L_vE_{26h}	0.86	96.79	109.38	0.50	−74.97
	$L_vE_S^{38v}$	0.88	50.24	57.75	0.85	−33.87
	$L_vE_S^{38h}$	0.87	48.47	55.68	0.86	−31.63
	$L_vE_S^{26v}$	0.80	49.68	55.06	0.83	−23.94
	$L_vE_S^{26h}$	0.93	57.28	71.26	0.81	−47.95
	$L_vE_K^{38v}$	0.84	48.29	54.24	0.85	−27.27
	$L_vE_K^{38h}$	0.84	46.71	52.36	0.86	−25.11
	$L_vE_K^{26v}$	0.77	47.91	52.96	0.83	−18.42
	$L_vE_K^{26h}$	0.89	55.34	66.76	0.81	−41.19
L_vE_{38v}	L_vE_{38h}	0.99	−3.76	18.54	0.98	4.99
	L_vE_{26v}	0.81	11.26	47.00	0.87	26.11
	L_vE_{26h}	0.95	28.99	51.78	0.78	−17.86
	L_vE_K	0.84	−55.93	113.38	0.56	87.12
	$L_vE_S^{38v}$	0.91	−5.77	38.82	0.92	22.83
	$L_vE_S^{38h}$	0.91	−7.57	41.43	0.91	24.97
	$L_vE_S^{26v}$	0.77	6.56	55.91	0.87	38.10
	$L_vE_S^{26h}$	0.90	7.91	43.38	0.86	12.09
	$L_vE_K^{38v}$	0.87	−5.18	43.71	0.92	29.98
	$L_vE_K^{38h}$	0.87	−6.55	46.57	0.91	32.04
	$L_vE_K^{26v}$	0.74	7.11	60.86	0.87	44.22
	$L_vE_K^{26h}$	0.86	8.25	46.40	0.86	19.64
$L_vE_S^{38v}$	$L_vE_S^{38h}$	0.99	−0.92	6.88	1.00	1.97
	$L_vE_S^{26v}$	0.91	1.48	22.25	0.98	11.14
	$L_vE_S^{26h}$	1.04	3.52	24.29	0.97	−9.03
	$L_vE_K^{38v}$	0.96	−0.32	7.72	1.00	5.38
	$L_vE_K^{38h}$	0.96	−1.09	10.96	1.00	7.28
	$L_vE_K^{26v}$	0.88	1.00	25.92	0.98	15.77
	$L_vE_K^{26h}$	1.00	3.09	22.60	0.97	−3.40
$L_vE_{EC}^{Res}$	L_vE_S	1.15	−5.22	40.70	0.90	−12.94
	L_vE_K	1.00	−21.82	50.58	0.83	22.09
	L_vE_{38v}	1.07	57.85	96.28	0.62	−66.92
	L_vE_{38h}	1.08	53.59	93.68	0.64	−63.89
	L_vE_{26v}	0.89	65.56	86.55	0.57	−52.75
	L_vE_{26h}	1.10	80.02	122.27	0.44	−92.92
	$L_vE_S^{38v}$	1.04	38.50	66.29	0.82	−43.42
	$L_vE_S^{38h}$	1.04	37.05	64.40	0.82	−41.25
	$L_vE_S^{26v}$	0.96	41.54	63.49	0.78	−36.59
	$L_vE_S^{26h}$	1.13	45.59	82.94	0.77	−59.61
	$L_vE_K^{38v}$	1.00	37.25	61.81	0.82	−37.11
	$L_vE_K^{38h}$	0.99	35.99	60.03	0.82	−35.02
	$L_vE_K^{26v}$	0.92	40.26	60.12	0.78	−31.26
	$L_vE_K^{26h}$	1.08	44.31	77.69	0.76	−53.12

underestimation when saturation occurred. A comparison of C_n^2 derived from both Kipp and Scintec on a linear scale showed an increasing deviation between the two scintillometers as C_n^2 increased (similar to Fig. 1 of Van Kesteren et al., 2015). Correspondingly, the bias between H_S and H_K or H_{EC} was also seen to increase with increasing H (Figs. 3 and 6).

In comparing the two different polarization of MW26 and MW38, H derived from v polarization of both MW26 or MW38 were found to be higher than those of their corresponding h polarization. As the horizontal and vertical components are subjected to different boundary conditions due to the low measurement height of the MWS systems, the differences observed in measurements from h and v polarizations may be caused by the outer scale effect. Turbulent eddies which are longer than the outer scale (often approximated as the measurement height) are no longer isotropic. Further studies will be required to explore the cause for these differences.

Comparisons of surface heat fluxes derived from the MWS of different frequencies showed that L_vE was the lowest for MW26v, followed by MW38h, MW38v and MW26h in increasing order (Fig. 7). Additionally, agreement between derived fluxes from MW26v and MW38v was better than that between MW26v and MW26h. The results are non-conclusive and may be related to several reasons including MW26 being more prone to absorption (Nieveen and Green, 1999). The wavelength selection is important because of its effect on the estimation of fluxes. The Fresnel zone, which is a function of wavelength, affects the requirements on the minimum measurement height. Moreover, while scintillometers with longer wavelengths (MW26) may cost less, they are less sensitive to scintillation (Eq. (1)) and more prone to water vapour absorption; this would have a greater effect on the data quality of MW26 than MW38 depending on the environment.

Comparisons of the resultant surface heat fluxes derived from the standalone method and the two-wavelength method provided an insight in the robustness of the iteration and minimization procedure applied in this study to solve for β of the standalone MWS. In comparison, the standalone MWS and two-wavelength method were more comparable, thereby demonstrating that a standalone MWS combined with the energy balance equation is able to solve for the same β as the two-wavelength method. However, referring to Sections 3.2.1 and 3.2.2, the standalone LAS performed

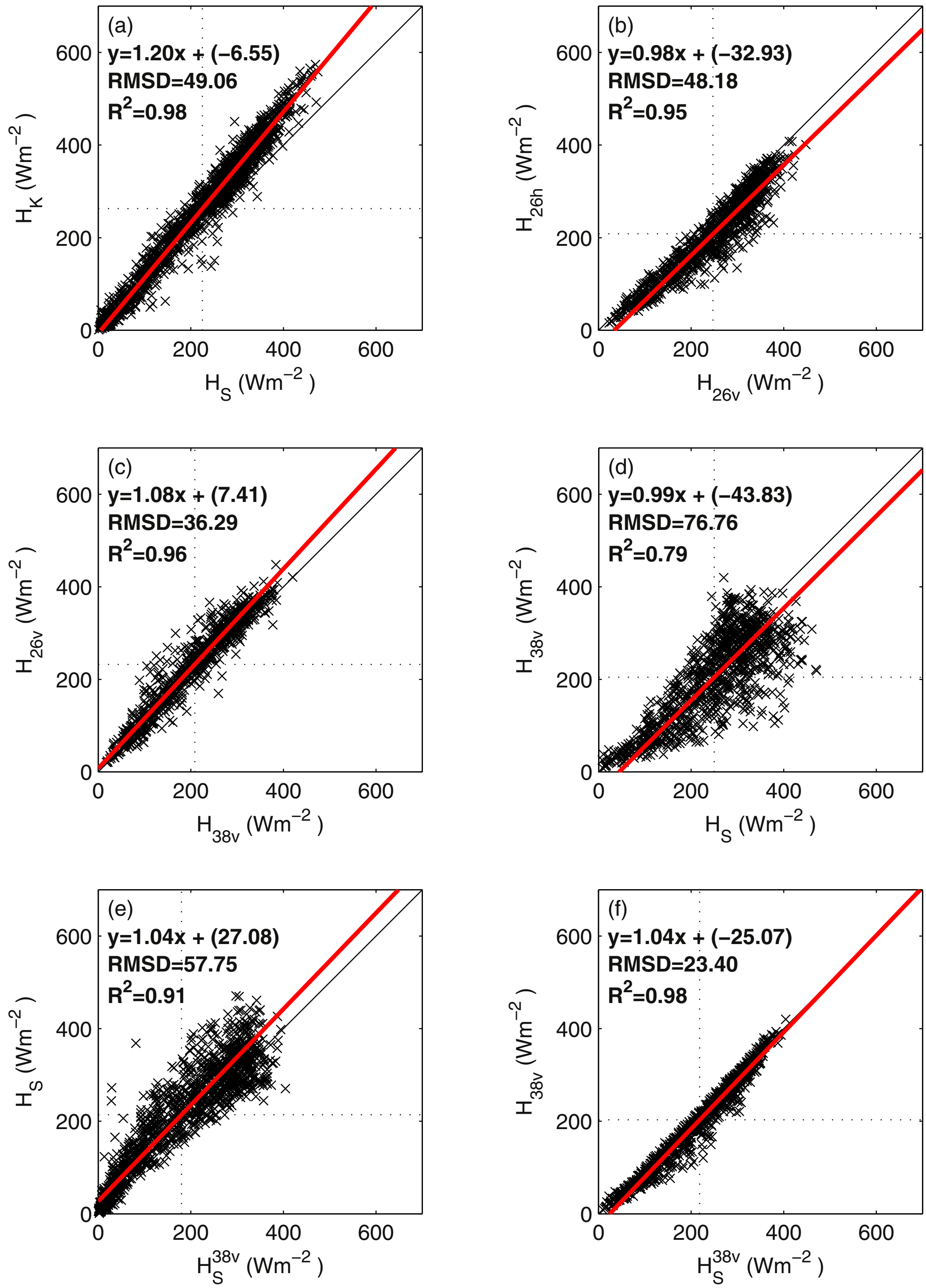

Fig. 6. Comparison of H derived from (a) Scintec and Kipp; (b) MW26v and MW26h; (c) MW38v and MW26v; (d) Scintec and MW38v; (e) Scintec – MW38v and Scintec; and (f) Scintec – MW38v and MW38v. Solid black line: 1:1 line. Solid red line: fitted line from orthogonal regression. Dotted black lines: mean H of each corresponding system. (For interpretation of the references to color in this figure legend, the reader is referred to the web version of this article.)

better in comparison to the standalone MWS and two-wavelength method.

Evans et al. (2010) have shown that r_{TQ} is important for an accurate derivation of L_vE for the two-wavelength method, while Wesely (1976) and Leijnse et al. (2007) have shown that uncertainties in r_{TQ} can cause large errors in the derived fluxes for dry conditions. Similarly, it can be observed that differences in H from a standalone LAS and the two-wavelength method increases with increasing magnitude of H. Therefore, despite the agreement between the standalone MWS and the two-wavelength method, a combination of dry conditions and the adopted value of r_{TQ} here may have contributed to the inaccuracy in the H and L_vE derived from these systems. Although using the bichormatic correlation method may help to improve the results here, the reduced sensitivity of scintillometers at high β may be a bigger issue (Ward et al., 2015).

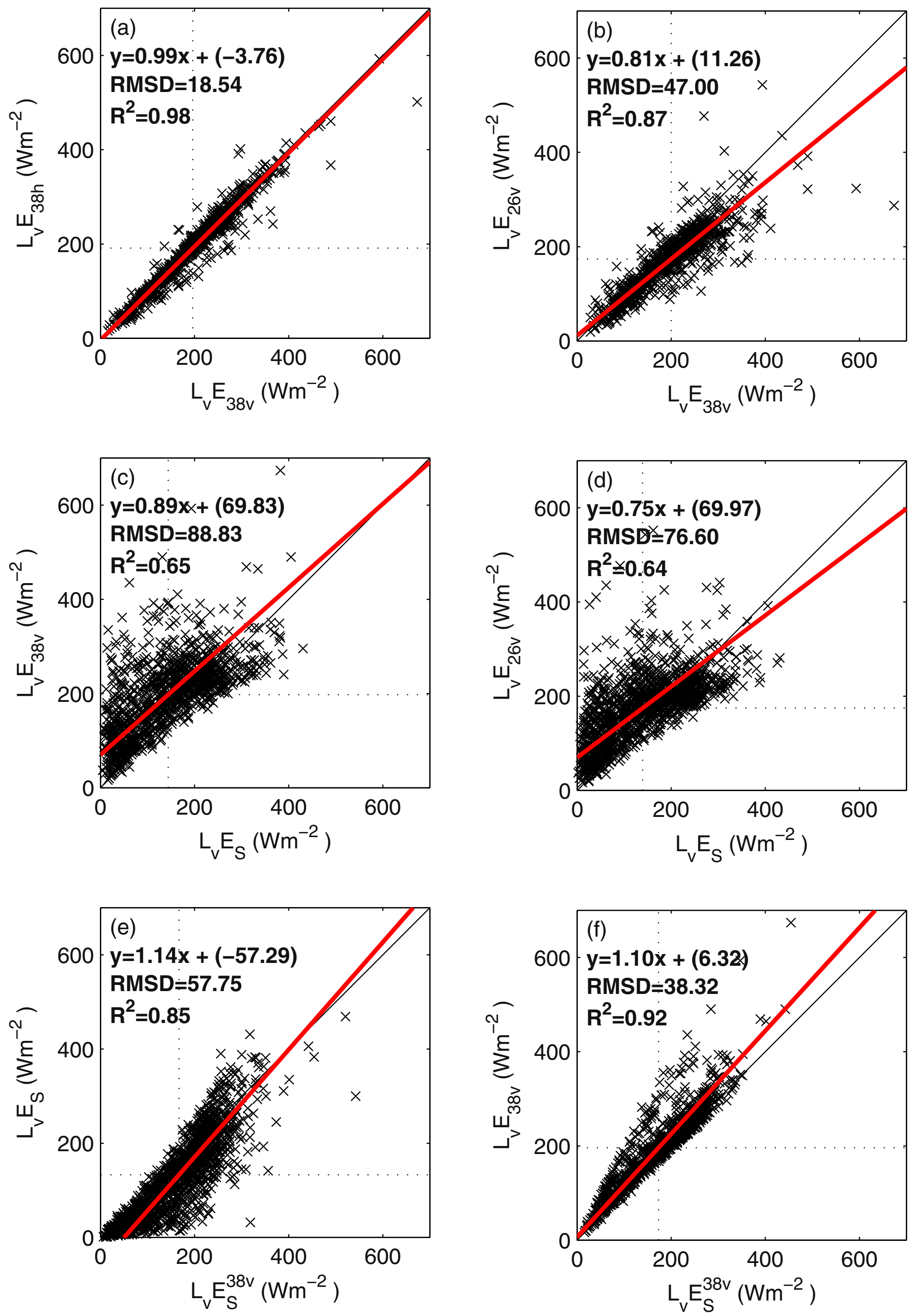

Fig. 7. Comparison of L_vE derived from (a) MW38v and MW38h; (b) MW38v and MW26v; (c) Scintec and MW38v; (d) Scintec and MW26v; (e) Scintec – MW38v and Scintec; and (f) Scintec – MW38v and MW38v. Solid black line: 1:1 line. Solid red line: fitted line from orthogonal regression. Dotted black lines: mean L_vE of each corresponding system. (For interpretation of the references to color in this figure legend, the reader is referred to the web version of this article.)

4. Conclusion

This study compared measurements of surface heat fluxes using an EC system, two LAS systems from two different manufacturers, and two MWS systems at different frequencies and polarizations and the two-wavelength method. Based on the results of this study, differences in H and L_vE may be caused by different theoretical principles of the different methods and uncertainty in parameters such as r_{TQ}, z_s, and h_0. Nevertheless, a standalone LAS combined with an energy budget constraint has been shown to be sufficient to derive both H and L_vE with an acceptable accuracy in a semi-arid environment.

In the case of MWS systems and the two-wavelength method, assumptions made regarding r_{TQ} were possibly the main cause for differences with the EC system. In the case of a standalone MWS, this uncertainty increased with increasing β due to the non-unique solution in β.

This study also compared the different types of scintillometers against each other. Based on comparisons of two LAS systems from different manufacturers, the need to correct for absorption as shown in previous studies was reinforced. Therefore, due to its in-built ability to correct for absorption, Scintec BLS900 is recommended for use.

The cause for differences between the two MWS of different frequencies has not been confirmed, but may be attributed to outer scale effect as a result of low measurement heights.

In conclusion, a standalone LAS is most suitable for applications in a semi-arid or dry environment as opposed to the two-wavelength method and standalone MWS method due to differences in their sensitivities at different site conditions (Ward et al., 2015).

Acknowledgements

This study was made possible through the provision of funding by JAXA (Specification no.: JX-PSPC-349279, Contract No.: 11RS-01707). M.S. Yee was supported by an Australian Postgraduate Award (APA) Scholarship. VRN Pauwels is currently funded by the Australian Research Council through the Future Fellowship scheme. The Faculty of Engineering from Monash University also supported this research through two seed grants. J. Beringer was funded under an ARC future fellowship (FT1110602). Support for collection and archiving was provided through the Australia Terrestrial Ecosystem Research Network (TERN) (http://www.tern.org.au). M.F. McCabe acknowledges support from the National Collaborative Research Infrastructure Strategy. Frank Winston, Tim Lubcke and Darren Hocking of Monash University are also acknowledged for their valuable contributions in the installation and maintenance of the flux tower and scintillometers, and finally, we are grateful to Hidde Leijinse for his inputs in the development of the program to solve the equations.

Appendix A. Calculation of fluxes from scintillometers

A brief description of the calculation of H and L_vE from C_n^2 measured by the scintillometers is presented here. We refer to Leijnse et al. (2007) for a comprehensive description of the derivations required for the calculation of these fluxes.

An iterative procedure using two loops was employed to calculate H and L_vE from the available measurements at 30-min intervals. From an initial guess of Bowen ratio, $\beta = H/L_vE$, H and L_vE were calculated as

$$H = \frac{\beta}{1+\beta}(R_n - G), \tag{A.1}$$

and

$$L_vE = \frac{1}{1+\beta}(R_n - G), \tag{A.2}$$

where R_n and G were measured or estimated from measured data.

An initial guess of u_* was then used to calculate L_{Ob} expressed as

$$L_{Ob} = -\frac{\rho u_*^3}{\kappa g\left[H/(c_pT) + 0.61(L_vE)/L_v\right]}, \tag{A.3}$$

where $c_p = 1005\,\mathrm{J\,kg^{-1}\,K^{-1}}$ is the specific heat of air at constant pressure, T is the air temperature, and κ is the von Kármán constant, assumed to equal 0.4. The density of moist air, ρ, is

$$\rho = \frac{p}{R_dT} - 0.61Q, \tag{A.4}$$

with R_d being the gas constant of dry air equal to $287.04\,\mathrm{J\,kg^{-1}\,K^{-1}}$. L_v is calculated as

$$L_v = 1000\cdot(2501 - 2.361\,(T - 273.15)). \tag{A.5}$$

A new value of u_* is then calculated from

$$u_* = \frac{\kappa u}{\ln((z_u-d_0)/z_0) - \Psi((z_u-d_0)/L_{Ob}) + \Psi(z_0/L_{Ob})}, \tag{A.6}$$

where u is wind speed at the height z_u and $\Psi(\cdot)$ is the Businger–Dyer function, expressed as

$$\Psi(y) = 2\ln\left(\frac{1+x}{2}\right) + \ln\left(\frac{1+x^2}{2}\right) - 2\arctan(x) + \frac{\pi}{2}, \tag{A.7}$$

with

$$x = (1-16y)^{1/4}. \tag{A.8}$$

Roughness length, z_0, and d_0 were calculated as

$$\begin{cases} z_0 = \dfrac{h_0}{8} \\ d_0 = \dfrac{2h_0}{3}. \end{cases} \tag{A.9}$$

The value of u_* calculated from Eq. (A.6) was compared to the guessed value; if the two were different, the new u_* was used in Eq. (A.3) and the procedure repeated until the difference between the initial u_* and that calculated with Eq. (A.6) became lower than 10^{-6}. This value of u_* was used to calculate the structure parameter of temperature, C_T^2, with the formula

$$C_T^2 = \frac{H^2}{\rho^2 c_p^2}\frac{1}{u_*^2(z_s-d_0)^{2/3}} f_{Ob}\left(\frac{z_s-d_0}{L_{Ob}}\right), \tag{A.10}$$

where z_s [m] is the effective beam height. For unstable conditions, the stability function, $f_{Ob}(.)$, can be written as

$$f_{Ob}(x) = c_1(1-c_2x)^{-2/3}, \tag{A.11}$$

with $c_1 = 4.9$ and $c_2 = 6.1$ (Andreas, 1989). The structure parameter of moisture, C_Q^2, was calculated as

$$C_Q^2 = \frac{L_vE^2}{L_v^2}\frac{1}{u_*^2(z_s-d_0)^{2/3}} f_{Ob}\left(\frac{z_s-d_0}{L_{Ob}}\right). \tag{A.12}$$

These were used to calculate C_n^2 with the expression

$$C_n^2 = A_T^2\frac{C_T^2}{T^2} + A_Q^2\frac{C_Q^2}{Q^2} + 2A_TA_Q\frac{C_{TQ}}{TQ}, \tag{A.13}$$

where the cross-structure parameter of temperature and humidity, C_{TQ}, is

$$C_{TQ} = r_{TQ}C_TC_Q, \tag{A.14}$$

with r_{TQ} assumed to equal 1.

The dimensionless sensitivity coefficients of the refractive index, A_T and A_Q, differ for LAS and MWS.

For LAS systems, they read

$$\begin{cases} A_{T_{LAS}} = m_1(\lambda)(\dfrac{P}{T}) - R_v m_2(\lambda)Q \\ A_{Q_{LAS}} = R_v m_2(\lambda)Q, \end{cases} \tag{A.15}$$

where R_v is the specific gas constant for water vapour ($461.5\,\mathrm{J\,K^{-1}\,kg^{-1}}$), $m_1(\lambda) = -0.27\times10^{-3}$ and $m_2(\lambda) = -0.70\times10^{-6}$ for typical atmospheric conditions ($P = 10^5$ Pa, $T = 288$ K, $Q = 0.012\,\mathrm{kg\,m^{-3}}$) (Andreas, 1989).

For the MWS systems, $A_{T_{MWS}}$ and $A_{Q_{MWS}}$ are

$$\begin{cases} A_{T_{MWS}} = -b\dfrac{p}{T} - c\dfrac{Q}{T} \\ A_{Q_{MWS}} = c\dfrac{Q}{T}, \end{cases} \tag{A.16}$$

where the constant b is equal to $0.776\cdot10^{-6}\,\mathrm{K\,Pa^{-1}}$, and the constant c is equal to $1.723\,\mathrm{K\,m^3\,kg^{-1}}$.

If the initial guess of β were correct, C_n^2 calculated from Eq. (A.13) would equal the measured C_n^2. In the case when the calculated and measured values of C_n^2 were different, a different guess of β should be used and the procedure should be repeated from Eq. (A.1). This gives a relationship between C_n^2 and β for given atmospheric conditions (measured P, T, Q, R_n, G, u). Using a minimization function, the β value which minimizes the difference between the scintillometer derived C_n^2 and $C_n^2(\beta)$ is found (i.e., $|C^2_{n_{measured}} - C_n^2(\beta)|$). The accuracy of β was set to 10^{-12}.

While the solution of this minimization is unique for LAS, each measured value of C_n^2 with MWS corresponded to two possible solutions of β (Leijnse et al., 2007). To find these two solutions, the minimum or turning point of $C_n^2(\beta)$, which is the lowest C_n^2 value possible based on the given atmospheric conditions, was first determined. Its corresponding β, herein referred to as $\beta_{\min}$, acts as a bound to the two possible β solutions; $\beta_{\min}$ was then used to limit the solver to solve for β for the given C_n^2 in the case where β was lower than $\beta_{\min}(0 < \beta < \beta_{\min})$ to derive β_1. Similarly, β_2 was derived in the case where β was between $\beta_{\min}$ and a large value, $\beta_{\max}$, which was assumed to be 30 ($\beta_{\min} < \beta < \beta_{\max}$). These solutions were then used to compute H and L_vE.

In the two-wavelength method, the same procedure was followed, with C_T^2 and C_Q^2 determined as (Hill et al., 1988)

$$\begin{cases} C_Q^2 = \dfrac{A^2_{T_{MWS}} C^2_{n_{LAS}} + A^2_{T_{LAS}} C^2_{n_{MWS}} + 2r_{TQ}\sqrt{C^2_{n_{MWS}} C^2_{n_{LAS}}}}{(T\Pi)^2} \\ C_T^2 = \dfrac{A^2_{Q_{MWS}} C^2_{n_{LAS}} + A^2_{Q_{LAS}} C^2_{n_{MWS}} + 2r_{TQ}\sqrt{C^2_{n_{MWS}} C^2_{n_{LAS}}}}{(Q\Pi)^2} \\ \Pi = \dfrac{A_{T_{MWS}} A_{Q_{LAS}} - A_{Q_{MWS}} A_{T_{LAS}}}{TQ}, \end{cases} \tag{A.17}$$

where, r_{TQ} was assumed to be 1.

References

Alfieri, J.G., Blanken, P.D., Smith, D., Morgan, J., 2009. Concerning the measurement and magnitude of heat, water vapor, and carbon dioxide exchange from a semiarid grassland. J. Appl. Meteorol. Climatol. 48 (5), 982–996, http://dx.doi.org/10.1175/2008JAMC1873.1

Andreas, E.L., 1989. Two-wavelength method of measuring path-averaged turbulent surface heat fluxes. J. Atmos. Ocean. Technol. 6 (2), 280–292, http://dx.doi.org/10.1175/1520-0426(1989)006<0280:TWMOMP>2.0.CO;2

Baghdadi, N., Cerdan, O., Zribi, M., Auzet, V., Darboux, F., El Hajj, M., Kheir, R.B., 2007. Operational performance of current synthetic aperture radar sensors in mapping soil surface characteristics in agricultural environments: application to hydrological and erosion modelling. Hydrol. Process. 22 (1), 9–20, http://dx.doi.org/10.1002/hyp.6609

Baldocchi, D., Falge, E., Gu, L., Olson, R., Hollinger, D., Running, S., Anthoni, P., Bernhofer, C., Davis, K., Evans, R., et al., 2001. FLUXNET: a new tool to study the temporal and spatial variability of ecosystem-scale carbon dioxide, water vapor, and energy flux densities. Bull. Am. Meteorol. Soc. 82 (11), 2415–2434, http://dx.doi.org/10.1175/1520-0477(2001)082<2415:FANTTS>2.3.CO;2

Beringer, J., Hutley, L.B., Tapper, N.J., Cernusak, L.A., 2007. Savanna fires and their impact on net ecosystem productivity in north Australia. Global Change Biol. 13 (5), 990–1004, http://dx.doi.org/10.1111/j.1365-2486.2007.01334.x

Beyrich, F., De Bruin, H., Meijninger, W., Schipper, J., Lohse, H., 2002. Results from one-year continuous operation of a large aperture scintillometer over a heterogeneous land surface. Boundary-Layer Meteorol. 105 (1), 85–97, http://dx.doi.org/10.1023/A:1019640014027

Beyrich, F., Kouznetsov, R.D., Leps, J.P., Lüdi, A., Meijninger, W.M.L., Weisensee, U., 2005. Structure parameters for temperature and humidity from simultaneous eddy-covariance and scintillometer measurements. Meteorol. Z. 14 (5), 641–649 http://www.ingentaconnect.com/content/schweiz/mz/2005/00000014/00000005/art00006

Brunsell, N., Ham, J., Arnold, K., 2011. Validating remotely sensed land surface fluxes in heterogeneous terrain with large aperture scintillometry. Int. J. Remote Sens. 32 (21), 6295–6314, http://dx.doi.org/10.1080/01431161.2010.508058

Chehbouni, A., Watts, C., Lagouarde, J.-P., Kerr, Y., Rodriguez, J.-C., Bonnefond, J.-M., Santiago, F., Dedieu, G., Goodrich, D., Unkrich, C., 2000. Estimation of heat and momentum fluxes over complex terrain using a large aperture scintillometer. Agric. Forest Meteorol. 105 (1), 215–226, http://dx.doi.org/10.1016/S0168-1923(00)00187-8

Evans, J., De Bruin, H., 2011. The effective height of a two-wavelength scintillometer system. Boundary-Layer Meteorol. 141 (1), 165–177, http://dx.doi.org/10.1007/s10546-011-9634-0

Evans, J., McNeil, D., Finch, J., Murray, T., Harding, R., Verhoef, A., 2010. Evaporation measurements at kilometre scales determined using two-wavelength scintillometry. In: BHS Third International Symposium: Role of Hydrology in Managing Consequences of a Changing Global Environment, Newcastle University, 19–23 July 2010, British Hydrological Society http://nora.nerc.ac.uk/21124/

Evans, J.G., Ph.D. thesis 2009, April. Long-path scintillometry over complex terrain to determine areal-averaged sensible and latent heat fluxes. The University of Reading http://nora.nerc.ac.uk/10410/

Ezzahar, J., Chehbouni, A., Hoedjes, J., Chehbouni, A., 2007. On the application of scintillometry over heterogeneous grids. J. Hydrol. 334 (34), 493–501 http://www.sciencedirect.com/science/article/pii/S0022169406005701

Ezzahar, J., Chehbouni, A., Hoedjes, J., Ramier, D., Boulain, N., Boubkraoui, S., Cappelaere, B., Descroix, L., Mougenot, B., Timouk, F., 2009. Combining scintillometer measurements and an aggregation scheme to estimate area-averaged latent heat flux during the AMMA experiment. J. Hydrol. 375 (1), 217–226, http://dx.doi.org/10.1016/S0168-1923(00)00187-8

Foken, T., 2008. The energy balance closure problem: an overview. Ecol. Appl. 18 (September (6)), 1351–1367, http://dx.doi.org/10.1890/06-0922.1

Fritschen, L., Qian, P., Kanemasu, E., Nie, D., Smith, E., Stewart, J., Verma, S., Wesely, M., 1992. Comparisons of surface flux measurement systems used in FIFE 1989. J. Geophys. Res.: Atmos. (1984–2012) 97 (D17), 18697–18713, http://dx.doi.org/10.1029/91JD03042

Green, A., Astill, M., McAneney, K., Nieveen, J., 2001. Path-averaged surface fluxes determined from infrared and microwave scintillometers. Agric. Forest Meteorol. 109 (3), 233–247, http://dx.doi.org/10.1023/A:1001730530267

Hartogensis, O., Watts, C., Rodriguez, J., De Bruin, H., 2003. Derivation of an effective height for scintillometers: La Poza experiment in Northwest Mexico. J. Hydrometeorol. 4 (5), 915–928, http://dx.doi.org/10.1175/1525-7541(2003)004<0915:DOAEHF>2.0.CO;2

Hemakumara, H., Chandrapala, L., Moene, A.F., 2003. Agric. Water Manag. 58 (2), 109–122 (Agricultural Water Management on Remote Sensing and Water Resources Management) http://www.sciencedirect.com/science/article/pii/S0378377402001312

Hendrickx, J.M., Kleissl, J., Vélez, J.D.G., Hong, S.-H., Duque, J.R.F., Vega, D., Ramírez, H.A.M., Ogden, F.L., 2007. Scintillometer networks for calibration and validation of energy balance and soil moisture remote sensing algorithms. Proc. SPIE 6565, http://dx.doi.org/10.1117/12.718124, 65650W–65650W-16.

Hill, R.J., Bohlander, R.A., Clifford, S.F., McMillan, R.W., Priestly, J., Schoenfeld, W., 1988. Turbulence-induced millimeter-wave scintillation compared with micrometeorological measurements. IEEE Trans. Geosci. Remote Sens. 26 (3), 330–342, http://dx.doi.org/10.1109/36.3035

Hornbuckle, J., Christen, E.W., 1999. In: Hornbuckle, J., Christen, E. (Eds.), Physical Properties of Soils in the Murrumbidgee and Coleambally Irrigation Areas. CSIRO Land and Water Canberra, A.C.T. http://nla.gov.au/nla.arc-13482

Hutley, L., Leuning, R., Beringer, J., Cleugh, H., 2005. The utility of the eddy covariance techniques as a tool in carbon accounting: tropical savanna as a case study. Aust. J. Bot. 53 (7), 663–675, http://dx.doi.org/10.1071/BT04147

Jung, M., Reichstein, M., Bondeau, A., 2009. Towards global empirical upscaling of FLUXNET eddy covariance observations: validation of a model tree ensemble approach using a biosphere model. Biogeosciences 6 (10), 2001–2013, http://dx.doi.org/10.5194/bg-6-2001-2009

Kaimal, J.C., Finnigan, J.J., 1994. Atmospheric Boundary Layer Flows: Their Structure and Measurement. Oxford University Press, New York.

Kite, G., Droogers, P., 2000. Comparing evapotranspiration estimates from satellites, hydrological models and field data. J. Hydrol. 229 (1), 3–18, http://dx.doi.org/10.1016/S0022-1694(99)00195-X

Kleissl, J., Watts, C., Rodriguez, J., Naif, S., Vivoni, E., 2009. Scintillometer intercomparison study-continued. Boundary-Layer Meteorol. 130 (3), 437–443, http://dx.doi.org/10.1007/s10546-009-9352-z

Kohsiek, W., 1982. Measuring C_T^2, C_Q^2, and C_{TQ} in the unstable surface layer, and relations to the vertical fluxes of heat and moisture. Boundary-Layer Meteorol. 24 (1), 89–107, http://dx.doi.org/10.1007/BF00121802

Kohsiek, W., Herben, M., 1983. Evaporation derived from optical and radio-wave scintillation. Appl. Opt. 22 (17), 2566–2570, http://dx.doi.org/10.1364/AO.22.002566

Lagouarde, J.-P., Bonnefond, J.-M., Kerr, Y., McAneney, K., Irvine, M., 2002. Integrated sensible heat flux measurements of a two-surface composite landscape using scintillometry. Boundary-Layer Meteorol. 105 (1), 5–35.

Lagouarde, J.-P., Irvine, M., Bonnefond, J.-M., Grimmond, C., Long, N., Oke, T., Salmond, J., Offerle, B., 2006. Monitoring the sensible heat flux over urban areas using large aperture scintillometry: case study of Marseille City during the escompte experiment. Boundary-Layer Meteorol. 118 (3), 449–476, http://dx.doi.org/10.1007/s10546-005-9001-0

Leijnse, H., Uijlenhoet, R., Stricker, J.N.M., 2007. Hydrometeorological application of a microwave link: 2. Precipitation. Water Resour. Res. 43 (4), W04417, http://dx.doi.org/10.1029/2006WR004989

Leuning, R., Van Gorsel, E., Massman, W.J., Isaac, P.R., 2012. Reflections on the surface energy imbalance problem. Agric. Forest Meteorol. 156, 65–74 http://www.sciencedirect.com/science/article/pii/S016819231100339X

Liu, S., Xu, Z., Zhu, Z., Jia, Z., Zhu, M., 2013. Measurements of evapotranspiration from eddy-covariance systems and large aperture scintillometers in the Hai

River Basin, China. J. Hydrol. 487, 24–38, http://dx.doi.org/10.1016/j.jhydrol.2013.02.025

Lüdi, A., Beyrich, F., Mätzler, C., 2005. Determination of the turbulent temperature-humidity correlation from scintillometric measurements. Boundary-Layer Meteorol. 117 (3), 525–550, http://dx.doi.org/10.1007/s10546-005-1751-1

Maayar, M.E., Chen, J.M., Price, D.T., 2008. On the use of field measurements of energy fluxes to evaluate land surface models. Ecol. Model. 214 (24), 293–304, http://dx.doi.org/10.1016/j.ecolmodel.2008.02.008

McJannet, D., Cook, F., McGloin, R., McGowan, H., Burn, S., 2011. Estimation of evaporation and sensible heat flux from open water using a large-aperture scintillometer. Water Resour. Res. 47 (5.), http://dx.doi.org/10.1029/2010WR010155

McJannet, D., Cook, F., McGloin, R., McGowan, H., Burn, S., Sherman, B., 2013. Long-term energy flux measurements over an irrigation water storage using scintillometry. Agric. Forest Meteorol. 168 (0), 93–107, http://dx.doi.org/10.1016/j.agrformet.2012.08.013

Meijninger, W., De Bruin, H., 2000. The sensible heat fluxes over irrigated areas in Western Turkey determined with a large aperture scintillometer. J. Hydrol. 229 (1), 42–49, http://dx.doi.org/10.1016/S0022-1694(99)00197-3

Meijninger, W., Green, A., Hartogensis, O., Kohsiek, W., Hoedjes, J., Zuurbier, R., De Bruin, H., 2002. Determination of area-averaged water vapour fluxes with large aperture and radio wave scintillometers over a heterogeneous surface Flevoland field experiment. Boundary-Layer Meteorol. 105 (1), 63–83, http://dx.doi.org/10.1023/A:1019640014027

Meijninger, W., Hartogensis, O., Kohsiek, W., Hoedjes, J., Zuurbier, R., De Bruin, H., 2002. Determination of area-averaged sensible heat fluxes with a large aperture scintillometer over a heterogeneous surface-Flevoland field experiment. Boundary-Layer Meteorol. 105 (1), 37–62, http://dx.doi.org/10.1023/A:1019647732027

Moncrieff, J., Clement, R., Finnigan, J., Meyers, T., 2005. Averaging, detrending, and filtering of eddy covariance time series. In: Lee, X., Massman, W., Law, B. (Eds.), Handbook of Micrometeorology, vol. 29 of Atmospheric and Oceanographic Sciences Library. Springer, Netherlands, pp. 7–31, http://dx.doi.org/10.1007/1-4020-2265-4_2

Natural Resources Advisory Council, N., 2010, October. Understanding our native grasslands: agricultural, environmental and indigenous values and management for the future, Tech. rep. State of New South Wales.

Nieveen, J., Green, A., 1999. Measuring sensible heat flux density over pasture using the C_T^2-profile method. Boundary-Layer Meteorol. 91 (1), 23–35, http://dx.doi.org/10.1023/A:1001730530267

Pauwels, V., Timmermans, W., Loew, A., 2008. Comparison of the estimated water and energy budgets of a large winter wheat field during AgriSAR 2006 by multiple sensors and models. J. Hydrol. 349 (3), 425–440, http://dx.doi.org/10.1016/j.jhydrol.2007.11.016

Samain, B., Defloor, W., Pauwels, V.R.N., Nov. 2011. Continuous time series of catchment-averaged sensible heat flux from a large aperture scintillometer: efficient estimation of stability conditions and importance of fluxes under stable conditions. J. Hydrometeor. 13 (2), 423–442, http://dx.doi.org/10.1175/JHM-D-11-030.1

Samain, B., Ferket, B.V.A., Defloor, W., Pauwels, V.R.N., 2011. Estimation of catchment averaged sensible heat fluxes using a large aperture scintillometer. Water Resour. Res. 47 (5), http://dx.doi.org/10.1029/2009WR009032

Samain, B., Simons, G.W., Voogt, M.P., Defloor, W., Bink, N.J., Pauwels, V., 2012. Consistency between hydrological model, large aperture scintillometer and remote sensing based evapotranspiration estimates for a heterogeneous catchment. Hydrol. Earth Syst. Sci. 16 (7), 2095–2107, http://dx.doi.org/10.1175/JHM-D-11-030.1

Savage, M., 2009. Estimation of evaporation using a dual-beam surface layer scintillometer and component energy balance measurements. Agric. Forest Meteorol. 149 (3–4), 501–517, http://dx.doi.org/10.1016/j.agrformet.2008.09.012

Smith, A.B., Walker, J.P., Western, A.W., Young, R.I., Ellett, K.M., Pipunic, R.C., Grayson, R.B., Siriwardena, L., Chiew, F.H.S., Richter, H., 2012. The Murrumbidgee soil moisture monitoring network data set. Water Resour. Res. 48 (7), http://dx.doi.org/10.1029/2012WR011976

Solignac, P., Brut, A., Selves, J., Béteille, J., Gastellu-Etchegorry, J., 2012. Attenuating the absorption contribution on C_n^2 estimates with a large-aperture scintillometer. Boundary-Layer Meteorol. 143 (2), 261–283, http://dx.doi.org/10.1007/s10546-011-9692-3

Stull, R.B., 1988. An Introduction to Boundary Layer Meteorology, vol. 13. Springer, http://dx.doi.org/10.1007/978-94-009-3027-8

Twine, T.E., Kustas, W., Norman, J., Cook, D., Houser, P., Meyers, T., Prueger, J., Starks, P., Wesely, M., 2000. Correcting eddy-covariance flux underestimates over a grassland. Agric. Forest Meteorol. 103 (3), 279–300, http://dx.doi.org/10.1016/S0168-1923(00)00123-4

Van Kesteren, B., 2012. Measuring Water-Vapour and Carbon-Dioxide Fluxes at Field Scales with Scintillometry (Sl: sn). http://edepot.wur.nl/239949

Van Kesteren, B., Beyrich, F., Hartogensis, O.K., Braam, M., 2015. Long-term evaluation of the Scintec boundary-layer scintillometer and the Wageningen large-aperture scintillometer: implications for scintillometer users. Boundary-Layer Meteorol., 1–21, http://dx.doi.org/10.1007/s10546-015-0023-y

Ward, H., Evans, J., Grimmond, C., 2014. Multi-scale sensible heat fluxes in the suburban environment from large-aperture scintillometry and eddy covariance. Boundary-Layer Meteorol. 152 (1), 65–89, http://dx.doi.org/10.1007/s10546-014-9916-4

Ward, H.C., Evans, J.G., Grimmond, C.S.B., 2013. Multi-season eddy covariance observations of energy, water and carbon fluxes over a suburban area in Swindon, UK. Atmos. Chem. Phys. 13 (9), 4645–4666 http://www.atmos-chem-phys.net/13/4645/2013/

Ward, H.C., Evans, J.G., Grimmond, C.S.B., 2015. Infrared and millimetre-wave scintillometry in the suburban environment – Part 2: Large-area sensible and latent heat fluxes. Atmos. Measur. Techn. 8 (3), 1407–1424 http://www.atmos-meas-tech.net/8/1407/2015/

Ward, H.C., Evans, J.G., Grimmond, C.S.B., Bradford, J., 2015. Infrared and millimetre-wave scintillometry in the suburban environment – Part 1: Structure parameters. Atmos. Measur. Techn. 8 (3), 1385–1405 http://www.atmos-meas-tech.net/8/1385/2015/

Webb, E.K., Pearman, G.I., Leuning, R., 1980. Correction of flux measurements for density effects due to heat and water vapour transfer. Q. J. R. Meteorol. Soc. 106 (447), 85–100, http://dx.doi.org/10.1002/qj.49710644707

Wesely, M.L., Jan 1976. The combined effect of temperature and humidity fluctuations on refractive index. J. Appl. Meteor. 15 (1), 43–49, http://dx.doi.org/10.1175/1520-0450(1976)015<0043:TCEOTA>2.0.CO;2

Wilson, K., Goldstein, A., Falge, E., Aubinet, M., Baldocchi, D., Berbigier, P., Bernhofer, C., Ceulemans, R., Dolman, H., Field, C., Grelle, A., Ibrom, A., Law, B., Kowalski, A., Meyers, T., Moncrieff, J., Monson, R., Oechel, W., Tenhunen, J., Valentini, R., Verma, S., 2002. Energy balance closure at FLUXNET sites. Agric. Forest Meteorol. 113 (14), 223–243 http://www.sciencedirect.com/science/article/pii/S0168192302001090

Zeweldi, D., Gebremichael, M., Wang, J., Sammis, T., Kleissl, J., Miller, D., 2010. Intercomparison of sensible heat flux from large aperture scintillometer and eddy covariance methods: field experiment over a homogeneous semi-arid region. Boundary-Layer Meteorol. 135 (1), 151–159, http://dx.doi.org/10.1007/s10546-009-9460-9.